AIMS Environmental Science

AIMS Environmental Science, 11(3): 444–456.
DOI: 10.3934/environsci.2024022
Received: 04 March 2024
Revised: 01 April 2024
Accepted: 05 June 2024
Published: 11 June 2024

http://www.aimspress.com/journal/environmental

Research article

A simulation study of CO_2 gas adsorption with bottom ash adsorbent from palm oil mill waste using computational fluid dynamic (CFD)

Novi Sylvia[1,*], Aden Syahrullah Tarigan[1], Rozanna Dewi[1], Yunardi Yunardi[2], Yazid Bindar[3], and Mutia Reza[4]

[1] Department of Chemical Engineering, Malikussaleh University, Lhokseumawe, 24351, Indonesia
[2] Department of Chemical Engineering, Syiah Kuala University, Banda Aceh, 23111, Indonesia
[3] Department of Chemical Engineering, Faculty of Industrial Technology, Institut Teknologi Bandung, Jl. Ganesha 10 Bandung 40132, Indonesia
[4] Department of Chemical Engineering, Institut Teknologi Kalimantan, Indonesia

*** Correspondence:** Email: novi.sylvia@unimal.ac.id; Tel: +628116846742.

Abstract: Biogas is a cost-effective, efficient, environmentally friendly, and renewable alternative energy source. While biogas contains CH_4, it also contains impurities in the form of 27–45% CO_2 gas. Therefore, it is necessary to purify biogas by removing CO_2 gas as it can reduce the calorific value of CH_4, the main component of biogas. The process of methane purification can be achieved through adsorption. Bottom ash, derived from palm oil mill waste, shows great potential for methane purification by effectively adsorbing CO_2. This research simulated the methane purification process using the computational fluid dynamics (CFD) method with the student version of the ANSYS R20 software. The study utilized an adsorbent made from bottom ash obtained from palm oil mill waste. The main objective was to investigate the performance of bottom ash as an adsorbent for removing CO_2 gas in a continuous gas flow within an adsorption column. The study involved varying the column bed height (4 cm, 8 cm, 12 cm) and gas flow rate (10 L/min, 15 L/min, 20 L/min). The results showed that the highest efficiency in removing CO_2 gas was 84.53% with a bed height of 12 cm and a flow rate of 10 L/min, while the lowest efficiency was 47.87% with a bed height of 4 cm and a flow rate of 20 L/min. Furthermore, the highest adsorption capacity for CO_2 gas was 1.64 mg/g with a bed height of 12 cm and a flow rate of 10 L/min, while the lowest capacity was 0.93 mg/g with a bed height of 4 cm and a flow rate of 20 L/min. The linearization of adsorption isotherm data indicated that the CO_2 gas adsorption process using bottom ash adsorbent followed the Langmuir model.

Keywords: adsorption; bottom ash; adsorption capacity; removal efficiency

Mathematics subject classification:

Magnitude	Unit	Description	Magnitude	Unit	Description
q_e	mg/g	Sorption capacity	ρ	Kg m^{-3}	Fluid density
C_0	g/L	Initial concentration	α	m^{-1}	Viscous resistance coefficient
C_e	g/L	Final concentration	t	sec	Time
m	g	Mass	u	m sec^{-1}	Gas velocity (x-direction)
V	L	Volume	v	m sec^{-1}	Gas velocity (y-direction)
C_2	m	Inertial resistance Coefficient	w	m sec^{-1}	Gas velocity (z-direction)
μ	Ns m^{-2}	Fluid viscosity	ε		Bed voidage fraction (Porosity)

1. Introduction

The rapid development of technology and population growth have led to a significant increase in energy demand. However, due to the limited availability of fossil energy sources, this can result in an energy crisis and unmet energy needs. An indication of this energy crisis is the recent scarcity of oil, such as kerosene, petrol, and diesel. This scarcity is a result of the high and ever-increasing fuel demand each year. As a consequence, the price of crude oil worldwide continues to rise annually. Resolving this conflict requires serious attention. Therefore, there is a need for alternative renewable energy sources that are cost-effective, efficient, and environmentally friendly [1].

One such alternative energy source that meets these criteria is biogas. Biogas is not only rich in methane gas, but also has a simple and environmentally friendly production process. It is produced through the fermentation of organic waste, such as garbage, food scraps, animal feces, and waste from the food industry. Methane gas (CH_4), carbon dioxide gas (CO_2), oxygen gas (O_2), hydrogen sulfide gas (H_2S), hydrogen gas (H_2), and other gases are the components of biogas. Among these elements, methane gas (CH_4) and carbon dioxide gas (CO_2) play a crucial role in determining the quality of biogas. A high content of CH_4 results in a high calorific value of the biogas, while a high content of CO_2 leads to a low calorific value. Therefore, in order to increase the calorific value of biogas, the CO_2 content must be removed [2,3].

Various methods have been employed to reduce CO_2 emissions, including physical and chemical absorption, cryogenics, membrane separation, microalgae bio-fixation, and adsorption. Among these methods, the sorption method that utilizes amine compounds is commonly used to separate the gas component from the gas mixture by passing it through a liquid. However, this separation process has its drawbacks, such as amine mixture degradation due to impurities in the gas phase at low temperatures (below 50°C), equipment corrosion, high energy requirements for regeneration, degradation of solvent quality due to impregnation with other products, and amine reduction through evaporation. Among these methods, the adsorption method stands out as the most favorable due to its economic viability, ability to remove organic matter, and absence of toxic side effects. Furthermore,

the adsorption method shows promise as an alternative for CO_2 sequestration, as it is relatively inexpensive, simpler, and does not produce liquid waste [4–6].

Removing CO_2 gas levels can be achieved using biosorbents made from boiler bottom ash. Palm oil mill boiler bottom ash is one type of adsorbent that can be used for gas purification because it contains carbon (C), oxygen (O), magnesium (Mg), aluminium (Al), silica (Si), phosphorus (P), sulfur (S), potassium (K), calcium (Ca), and iron (Fe). However, the primary components are carbon (C), oxygen (O), and silica (Si). It has been discovered that bottom ash contains the silica oxide (SiO_2) compound, which has demonstrated excellent activity in the CO_2 adsorption process [7–10].

Studying the adsorption process of CO_2 is of great interest, both experimentally and through simulation. Computational fluid dynamics (CFD) is a simulation method that is known for its cost-effectiveness and ability to validate experimental data. CFD is a field within fluid mechanics that employs numerical methods and algorithms to solve and analyze problems related to fluid flow, heat transfer, and chemical reactions through computer simulations [7,11].

Building upon the aforementioned information, this research involves adsorption utilizing a fixed-bed column system with adsorbents created from palm oil mill boiler waste, specifically bottom ash. Computational fluid dynamics (CFD) with Ansys 2020 R2 commercial software was employed in this study. CO_2 gas was introduced into the fixed-bed column, with a predetermined CO_2 composition. The height of the adsorbent bed and the incoming gas flow rate were varied. Figure 1 illustrates the research scheme. The simulation results were analyzed, and the impact of separation factors under different conditions was calculated. The objective of this study was to analyze the influence of bed height and the incoming gas flow rate on sorption capacity, sorption efficiency, and adsorption isotherms [8].

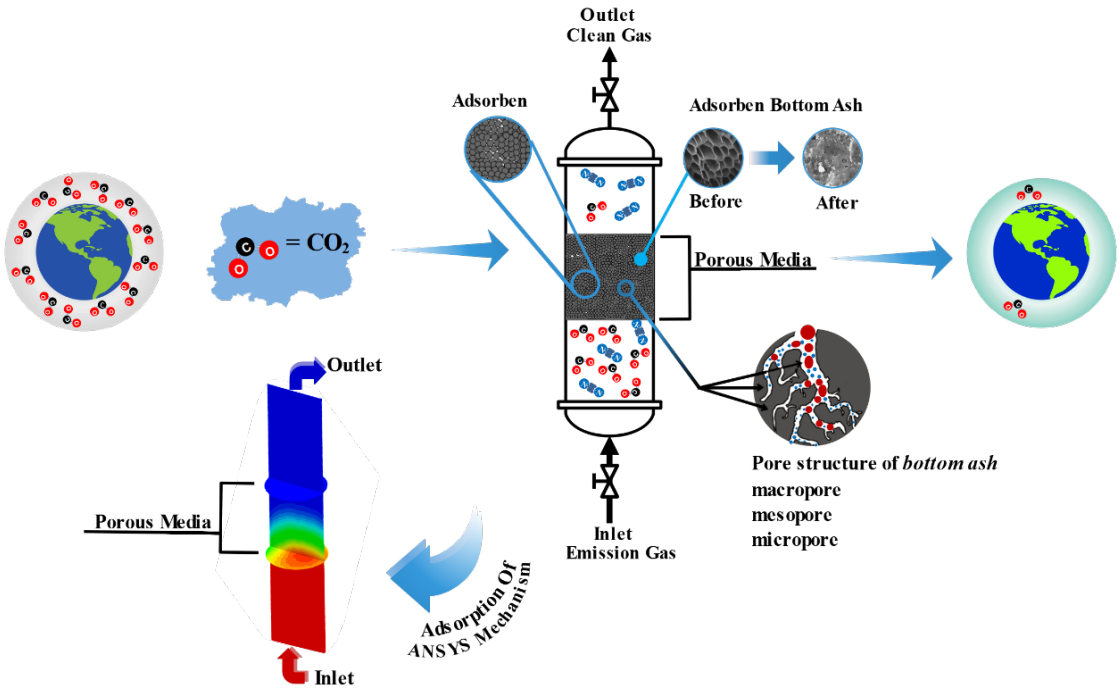

Figure 1. The mechanism of fixed-bed column simulation in ANSYS.

2. Research and method

2.1. Model geometry

The 3-D model geometry for the simulation in this study was developed with the help of design modeling using the application integrated in ANSYS Fluent. This was used to model a fixed-bed column to analyse the dynamic behavior of the adsorption process. For this study, the length of the cylinder was fixed at a 30-cm height and 6.4-cm diameter. The 3-D design for the fixed-bed column is illustrated in Figure 2. The boundary conditions of the study are shown in Figure 3.

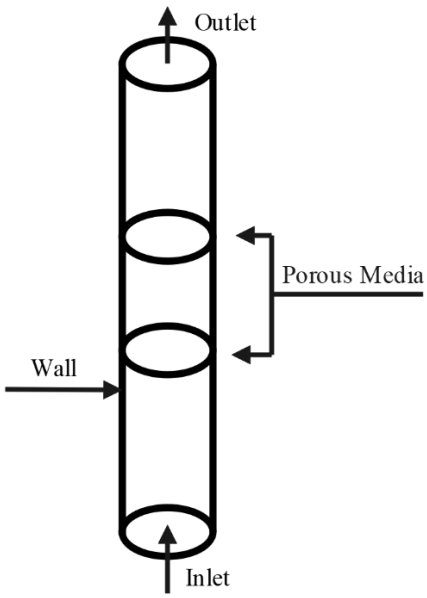

Figure 2. The fixed-bed column geometry.

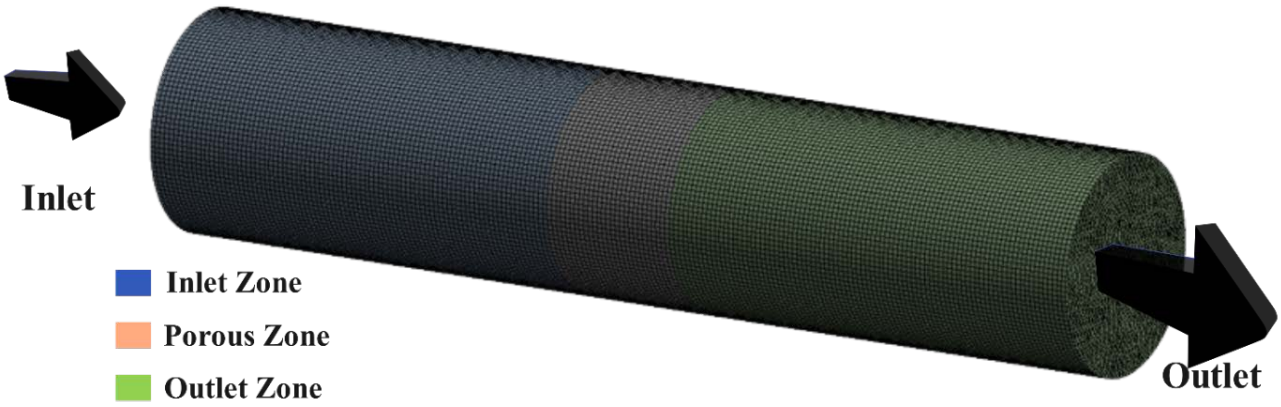

Figure 3. The boundary condition geometry.

2.1.1 Mesh generation

Before conducting simulations on the fixed-bed column geometry, it is crucial to determine the mesh value as it significantly impacts the generated cells. The assessment of mesh quality is carried

out to identify the appropriate mesh size that balances computation time and result accuracy [12]. The accuracy value can be seen in Figure 4. As for this study, when viewed from the quality of the mesh through the scewness mess metrics spectrum, the quality value is obtained in the range of 0.00049633–0.355 with a total shell of 600,000. The mesh method used in this study is multizone with a prism mesh type. From the value range obtained before entering the post-processing stage, the mesh geometry value prepared is classified as very good. For a view of the fixed-bed column geometry at the mesh stage, see Figure 5.

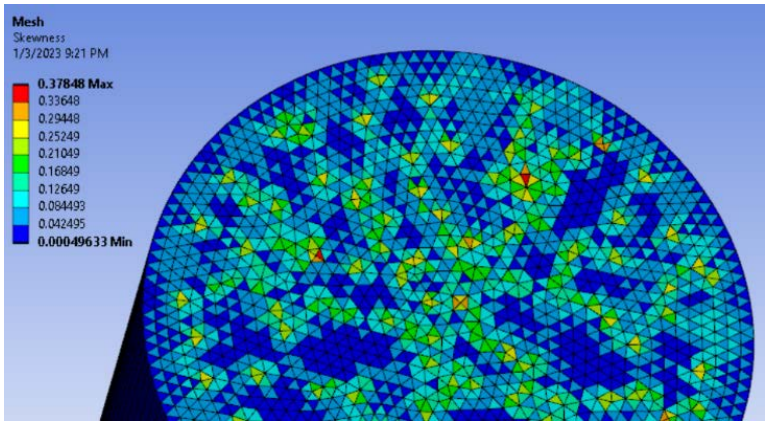

Figure 4. The mesh value of the fixed-bed column geometry**.**

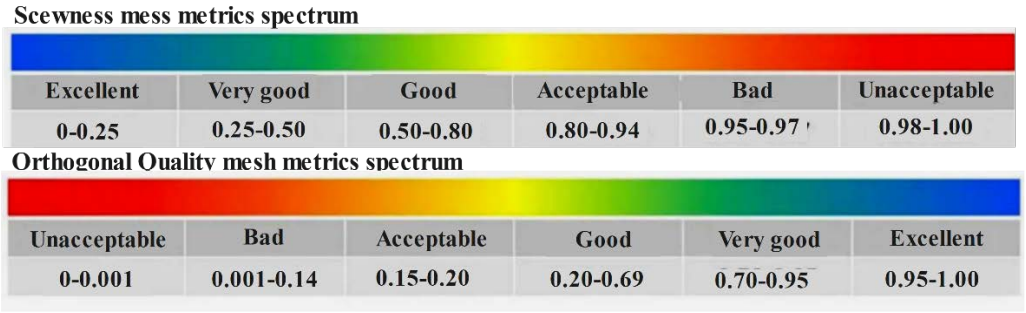

Figure 5. The validity of the mesh quality.

2.2. Mathematical model

The dynamic process of an adsorption column can be modeled and characterized using an integrated CFD model. To formulate a general adsorption model to fit the adsorption mechanism, the following assumptions are made [6]:

- Heat transfer within the bed is negligible;
- Competitive adsorption between CO_2 and N_2 is assumed with a mixtures model to represent mass transfer into the bed pellets;
- The mass transfer coefficient is equated to the external fluid film resistance and macropore diffusion;
- Porosity is uniform and constant;
- The equation used in the adsorption column is the continuity equation.

The generalized 3-D continuity equation for unsteady-state fluid flow is shown in Eq 1 [11,13,14]:

$$\frac{\partial \rho}{\partial t}+\frac{\partial \rho u}{\partial x}+\frac{\partial \rho v}{\partial y}+\frac{\partial \rho w}{\partial z}=0 \tag{1}$$

The Navier-Stokes equations for fluid flow through porous media where heat sources S_{ix}, S_{iy}, and S_{iz} are added to Eqs 2–4 to model flow resistance in 3-D dimensions [12,15] are:

Navier-Stokes equation in the *x*-direction

$$\begin{aligned}&\frac{\partial(\rho u)}{\partial t}+\frac{\partial(\rho uu)}{\partial x}+\frac{\partial(\rho vu)}{\partial y}+\frac{\partial(\rho wu)}{\partial z}=-\frac{\partial P}{\partial x}+2\frac{\partial}{\partial x}(\mu\frac{\partial u}{\partial x})\\&-\frac{2}{3}\frac{\partial}{\partial x}\left[\mu\left(\frac{\partial u}{\partial x}+\frac{\partial v}{\partial y}+\frac{\partial w}{\partial z}\right)\right]+\frac{\partial}{\partial y}\left[\mu\left(\frac{\partial u}{\partial y}+\frac{\partial v}{\partial x}\right)\right]+\frac{\partial}{\partial z}\left[\mu\left(\frac{\partial u}{\partial z}+\frac{\partial w}{\partial x}\right)\right]+S_{ix}\end{aligned} \tag{2}$$

Navier-Stokes equation in the *y*-direction

$$\begin{aligned}&\frac{\partial(\rho v)}{\partial t}+\frac{\partial(\rho vv)}{\partial y}+\frac{\partial(\rho uv)}{\partial x}+\frac{\partial(\rho wv)}{\partial z}=\frac{\partial P}{\partial y}+2\frac{\partial}{\partial y}\left(\mu\frac{\partial v}{\partial y}\right)\\&-2\frac{\partial}{\partial y}\left[\mu\left(\frac{\partial u}{\partial x}+\frac{\partial v}{\partial y}+\frac{\partial w}{\partial z}\right)\right]+\frac{\partial}{\partial x}\left[\mu\left(\frac{\partial v}{\partial x}+\frac{\partial u}{\partial y}\right)\right]+\frac{\partial}{\partial z}\left[\mu\left(\frac{\partial v}{\partial z}+\frac{\partial w}{\partial y}\right)\right]+S_{iy}\end{aligned} \tag{3}$$

Navier-Stokes equation in the *z*-direction

$$\begin{aligned}&\frac{\partial(\rho w)}{\partial t}+\frac{\partial(\rho ww)}{\partial z}+\frac{\partial(\rho uw)}{\partial x}+\frac{\partial(\rho vw)}{\partial y}=\frac{\partial P}{\partial z}+2\frac{\partial}{\partial z}\left(\mu\frac{\partial w}{\partial z}\right)\\&-\frac{2}{3}\frac{\partial}{\partial z}\left[\mu\left(\frac{\partial u}{\partial x}+\frac{\partial v}{\partial y}+\frac{\partial w}{\partial z}\right)\right]+\frac{\partial}{\partial x}\left[\mu\left(\frac{\partial w}{\partial x}+\frac{\partial u}{\partial z}\right)\right]+\frac{\partial}{\partial y}\left[\mu\left(\frac{\partial w}{\partial y}+\frac{\partial v}{\partial z}\right)\right]+S_{iz}\end{aligned} \tag{4}$$

The S_i porous media momentum source can calculate the pressure gradient in the packed bed and generate a pressure drop proportional to the fluid velocity, as shown in Eq 5 [12]:

$$S_i=\frac{\mu}{\alpha}\mu_i+C_2\left(\frac{1}{2}\rho u_i|u_i|\right) \tag{5}$$

where

$$C_2=\frac{1.75}{D_p}\frac{(1-\varepsilon)}{\varepsilon^3} \tag{6}$$

$$\alpha=\frac{D_p^2}{150}\frac{\varepsilon^3}{(1-\varepsilon)^2} \tag{7}$$

where C_2 and α are the inertial resitance and viscous resitance, which are estimated by Eqs 6 and 7. We can calculate the percent absorption and absorption capacity (q_e) using the following Eq 8 [7]:

$$q_e=\frac{(C_0-C_e)V}{m} \tag{8}$$

$$removal\ \%=\frac{(C_0-C_e)}{C_0} \tag{9}$$

where q_e is the amount of heavy metal adsorbed (mg/g), C_0 and C_e are the initial and final

concentrations of gas, respectively, *V* is the volume of solution (L), and *m* is the mass of adsorbent (g).

2.3. Boundary conditions

The adsorbent material used in this study is bottom ash, with a particle size of 46 μm. The gas employed is a mixture of CO_2 and N_2, with variable flow rates when passed through the fixed-bed column. The experimental procedure is outlined in Figure 1. The mole fraction of CO_2 and N_2 in the gas mixture is 95% and 5%, respectively. The system operates at a pressure of 1 atm and a temperature of 25 °C. Detailed specifications for the gas flow rate and bed height are provided in Tables 1 and 2.

Table 1. Simulation data of the adsorption process.

Operating Conditions	Value
Inlet gas flow rate (L/min)	10, 15, 20
Bed height (cm)	4, 8, 12
Inlet gas composition	95 % CO_2; 5 % N_2
Column height (cm)	30
Porosity, ε	0.88

Table 2. The spatial discretization schemes.

Variabel	Discrete scheme
Pressure-velocity coupling	Coupled
Pressure	Presto
Density	Quick
Momentum	Second order upwind
Species	Second order upwind
Energy	Second order upwind

3. Results

3.1. The effect of bed height and flow rate on CO_2 removal efficiency

The impact of flow rate on CO_2 removal efficiency is illustrated in Figure 6(a). The findings demonstrate that a higher flow rate corresponds to a lower CO_2 removal efficiency. This is attributed to the fact that a higher CO_2 gas flow rate reduces the contact time between CO_2 and the adsorbent, thereby leading to a decrease in the percentage of CO_2 removal efficiency [16–18]. Similar findings were also observed in a study conducted by Dupre et al. [19], wherein the flow rate significantly influenced the results of CO_2 gas absorption. Decreasing the flow rate extends the breakthrough time. By employing a low flow rate, an extended breakthrough time can be achieved, which in turn enhances the contact time and mass transfer of CO_2 gas or the diffusion process on the adsorbent [11].

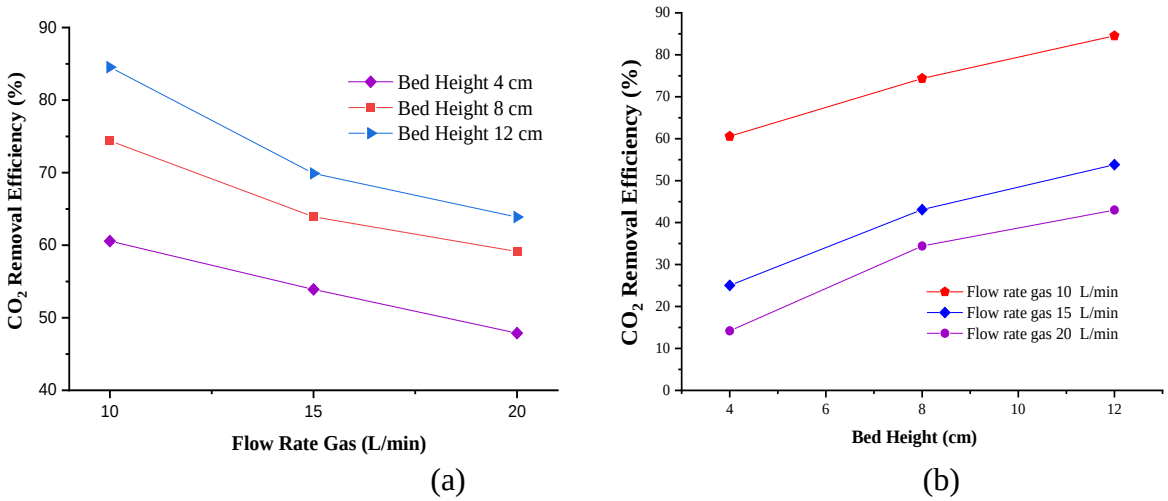

Figure 6. The effect of flow rate (a) and bed height (b) on CO_2 removal efficiency.

Based on Figure 6(b), it is evident that as the height of the adsorbent bed in the adsorption column increases, the efficiency of CO_2 removal also increases. This correlation can be attributed to the surface area and active sites of the adsorbent, where taller beds provide a larger surface area and greater adsorption capacity. Additionally, the highest bed contains a larger quantity of adsorbent particles, thereby facilitating enhanced contact between the solid and CO_2 gas as it flows through the column [14]. A higher height of the bed can increase the contact time or delay the breakthrough time of the adsorbent, which means the bed is able to be operated for a longer period of time without changing the type of adsorbent being used. Instead, for a lower bed, the breakthrough time will increase or approach faster. Therefore, the performance decreases [4]. The results of this study can be seen in Figures 6 and 7, where the highest CO_2 removal efficiency was obtained in a bed with a height of 12 cm by 84.53% with a flow rate of 10 L/min, while the lowest CO_2 removal efficiency was obtained 47.87% in a bed with a height of 4 cm with a flow rate of 20 L/min [16,17].

3.2 The effect of flow rate and bed height on CO_2 adsorption capacity

Based on Figure 7 (a), (b), it is evident that the flow rate has an impact on the adsorption capacity of CO_2 gas. Specifically, when the flow rate in the adsorption column is higher, the absorption capacity of CO_2 gas decreases. This can be attributed to the fact that increasing the flow rate reduces the contact time and mass transfer between the adsorbent and CO_2. Additionally, a higher flow rate reduces the amount of time the adsorbate (CO_2) spends within the adsorbent, leading to a lower adsorption capacity for CO_2 gas. Conversely, decreasing the flow rate of the incoming gas enhances the contact time and mass transfer between the adsorbent and CO_2. In other words, a lower flow rate within the adsorption column allows for a longer residence time of CO_2 molecules, leading to a higher amount of CO_2 being adsorbed and more time for the adsorbate (CO_2) to be absorbed by the adsorbent. Ultimately, this results in an increased CO_2 adsorption capacity [1]. The highest adsorption capacity was obtained at a flow rate of 10 L/min with a bed height of 12 cm with an adsorption capacity of 1.64 mg/g, while the lowest adsorption capacity was at a rate of 20 L/min with a bed height of 4 cm with an absorption capacity of 0.93 mg/g [3,6,18–21].

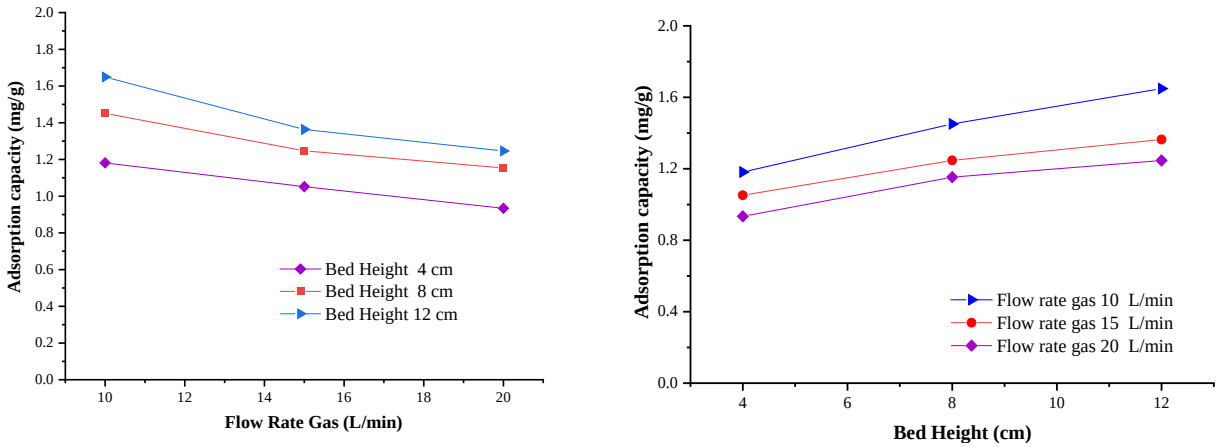

Figure 7. The effect of flow rate and bed height on CO_2 gas absorption capacity.

3.3. The contour of CO_2 removal by the simulation result

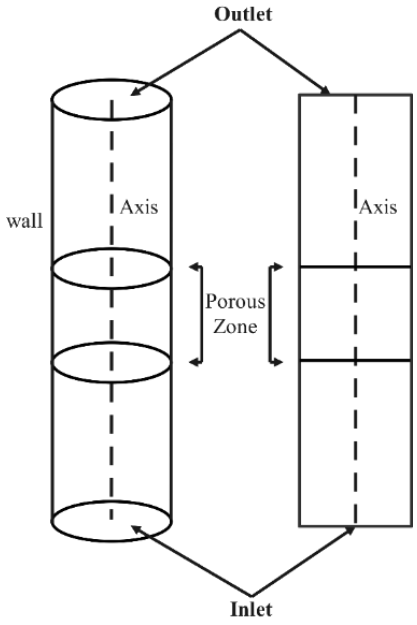

Figure 8. The skema fixed-bed column.

The simulated fixed-bed column was made with a cylindrical geometry, with the flow entering evenly from the bottom and exiting at the top during the adsorption process [7,17]. Figure 8 shows the schematic geometry of the fixed-bed column, shaft zone, and gas mixture inflow and outflow. A two-dimensional (2-D) axisymmetric CFD model was created to view the contours of concentration and velocity in the fixed-bed column, which can be seen in Figure 9 for concentration and Figure 10 for velocity.

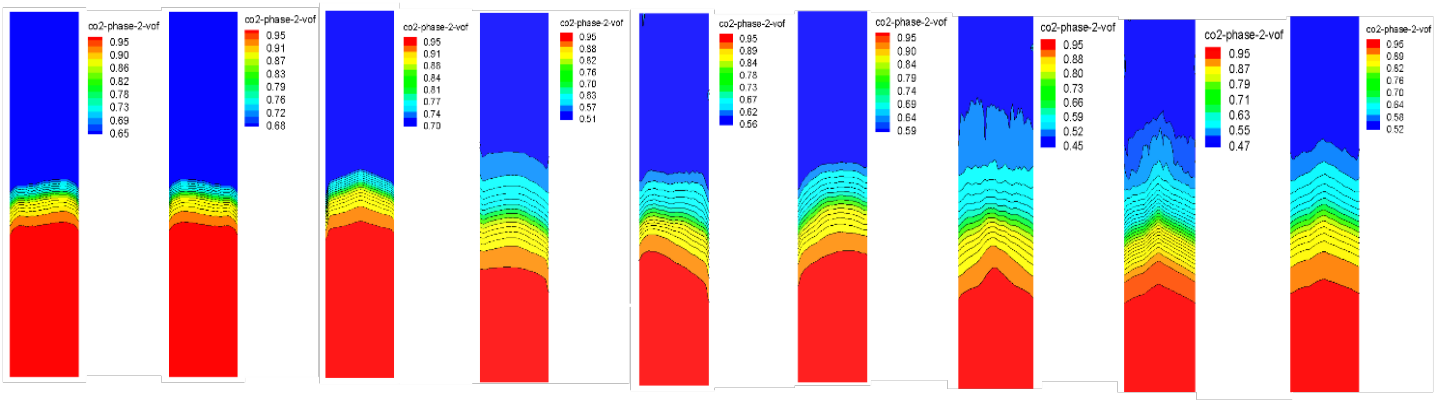

(a) (b) (c) (d) (e) (f) (g) (h) (i)

Figure 9. The contours of CO_2 concentration distribution with flow rate and bed height: (a) 10 L/m at 4 cm, (b) 15 L/m at 4 cm, (c) 20 L/m at 4 cm, (d) 10 L/m at 8 cm, (e) 15 L/m at 8 cm, (f) 20 L/m at 8 cm, (g) 10 L/m at 12 cm, (h) 15 L/m at 12 cm, and (i) 20 L/m at 12 cm.

Based on Figure 9, it is evident that the contour results show a significant decrease in CO_2 gas concentration when passing through the bottom ash adsorbent. Figure 10 illustrates the changes in concentration that occur in the porous zone. In this zone, a portion is visualized as an adsorbent bed that is responsible for absorbing CO_2 gas. The decrease in concentration is a result of the CO_2 gas being absorbed through the contact between CO_2 and bottom ash. This absorption process takes place in the porous zone area, which has a surface area of 0.93 m2/g and a pore volume of 0.12 cm3/g [3,10,19,22]. Bottom ash has 3 types of pores, namely, macropore (55 nm and > 55 nm), mesopore (7 nm and 8 nm), and micropore (< 1 nm) [4,6,8,9,16,17,20]. Gas adsorption capability is dependent on the texture of the adsorbent. CO_2 gas adsorption requires adsorbents with micropore size (<1 nm) because the gas has a small molecular size of <4 nm. The decrease in CO_2 gas concentration in the porous zone also occurs because it is dependent on Vanderwaals interactions related to the polarity of adsorbate and adsorbent molecules [5,7,9,10,13,15,18,20,21].

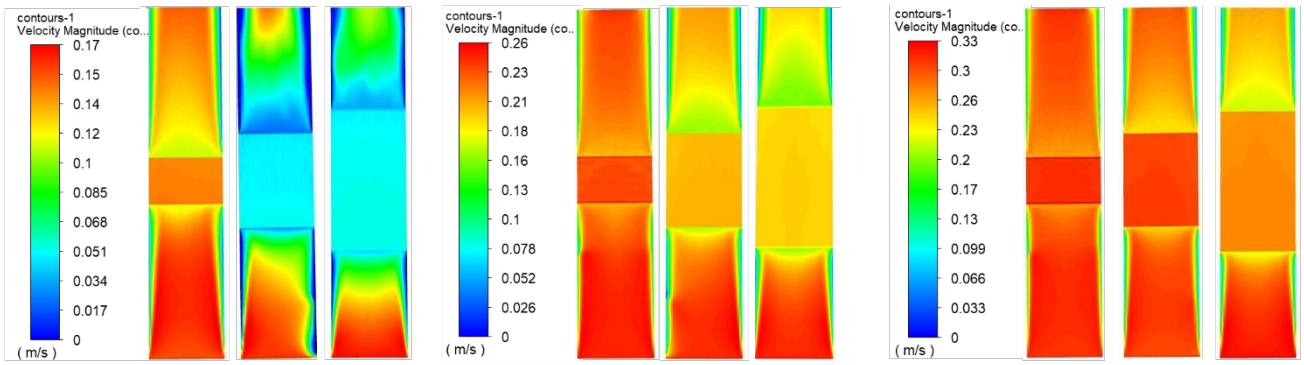

(a) (b) (c) (d) (e) (f) (g) (h) (i)

Figure 10. CO_2 velocity contours with flow rate and bed height: (a) 10 L/m at 4 cm, (b) 10 L/m at 8 cm, (c) 10 L/m at 12 cm, (d) 15 L/m at 4 cm, (e) 15 L/m at 8 cm, (f)15 L/m at 12 cm, (g) 20 L/m at 4 cm, (h) 20 L/m at 8 cm, and (i) 20 L/m at 12 cm.

Based on the contours results in Figure 10, it can be seen that the higher the bed, the lower the CO_2 velocity. The decrease in velocity in the bed section is because the greater the gas velocity, the greater the pressure drop that occurs [9,11–13,15–17,21,23].

3.4. Adsorption isotherms

According to Table 3 of the Langmuir isotherm, the R^2 value is 0.995, the *qm* value is 0.567, and the Langmuir constant is -2.694. In contrast, the Freundlich isotherm yields an R^2 value of 0.965. Based on the obtained *y*-value, the *n*-value is -1.19, and the Freundlich constant is 11.74. By comparing the determination values of *R* in the Langmuir isotherm and the Freundlich isotherm, this study suggests that the bonding of CO_2 with the bottom ash adsorbent follows the Langmuir model. This indicates that the absorption process occurs in a monolayer, as supported by the coefficient of determination *R* being closest to 1 [1,2,4,7,12,13,16,18,21].

Table 3. The adsorption isotherm model at 1 atm pressure and 25 °C temperature.

Type	Equation Nonliner	Linear
Langmuir		
q	0.567	$q = \frac{q_m \times k_L \times C_e}{1 + k_L \times C_e}$	$\frac{C_e}{q} = \frac{1}{q_m \times k_L} + \frac{C_e}{q_m}$
k	-2.694	
R	0.995	
Freundlich		
k	11.74	$q = k \times C_e^{\frac{1}{n}}$	$\log q = \log k + \frac{1}{2}\log C_e$
n	-1.19	
R	0.965	

3. Conclusions

The study found that increasing the height of the bed resulted in higher efficiency and capacity for removing CO2 gas. However, as the flow rate increased, the efficiency and capacity decreased. The highest CO2 gas removal efficiency was 84.53% with a bed height of 12 cm and a flow rate of 10 L/min, while the lowest was 47.87% with a bed height of 4 cm and a flow rate of 20 L/min. Similarly, the highest CO2 gas adsorption capacity was 1.64 mg/g with a bed height of 12 cm and a flow rate of 10 L/min, and the lowest was 0.93 mg/g with a bed height of 4 cm and a flow rate of 20 L/min. The results also showed that the adsorption process using bottom ash as an adsorbent following the Langmuir model, indicating that it occurred in a monolayer manner. Bottom ash, a waste product from palm oil mill boilers, can be used as an alternative adsorbent for CO2 adsorption. In future research, a fixed-bed column system and bottom ash from palm oil mills could be used for CO2 adsorption from biogas.

Use of AI tools declaration

The authors declare they have not used Artificial Intelligence (AI) tools in the creation of this article.

Acknowledgments

The authors are grateful to Malikussaleh university of chemical engineering simulation and process laboratory team

Conflict of interest

The authors have no conflicts of interest to declare.

References

1. Li H, Tan Y, Ditaranto M, et al. (2017) Capturing CO_2 from biogas plants. *Energy procedia* 114: 6030-6035. https://doi.org/10.1016/j.egypro.2017.03.1738
2. Li M, Zhu Z, Zhou M, et al. (2021) Removal of CO_2 from biogas by membrane contactor using PTFE hollow fibers with smaller diameter. *J Membr Sci* 627: 119232. https://doi.org/10.1016/j.memsci.2021.119232
3. Oyedeji OA (2019) Understanding and modeling the formation of syngas contaminants during biomass gasification, University of Tennessee
4. Cho YM, Yang YM, Park DS, et al. (2013) Study on CO_2 adsorption on LiOH-modified Al_2O_3. *Appl Mech Mater* 284: 342-346. https://doi.org/10.4028/www.scientific.net/AMM.284-287.342.
5. Ochedi FO, Liu Y, Adewuyi YG (2020) State-of-the-art review on capture of CO_2 using adsorbents prepared from waste materials. *Process Saf Environ* 139: 1-25 https://doi.org/10.1016/j.psep.2020.03.036.
6. Chen Q, Rosner F, Rao A, et al. (2019) Simulation of elevated temperature solid sorbent CO_2 capture for pre-combustion applications using computational fluid dynamics. *Appl energy* 237: 314-325. https://doi.org/10.1016/j.apenergy.2019.01.042
7. Pham TD, Xiong R, Sandler SI, et al. (2014) Experimental and computational studies on the adsorption of CO_2 and N_2 on pure silica zeolites. *Microporous Mesoporous Mater* 185: 157-166. https://doi.org/10.1016/j.micromeso.2013.10.030
8. Sylvia N, Fitriani F, Dewi R , et al. (2021) Characterization of bottom ash waste adsorbent from palm oil plant boiler burning process to adsorb carbon dioxide in a fixed bed column. *Indones J Chem* 21: 1454-1462. https://doi.org/10.22146/ijc.66509
9. Sethupathi S, Chung LL, Younas M, et al. (2017) Gaseous pollutant removal using solid wastes adsorbents," in : *Air, Gas, and Water Pollution Control Using Industrial and Agricultural Solid Wastes Adsorbents*: CRC Press, 3-20.
10. Promraksa A, Rakmak N (2020) Biochar production from palm oil mill residues and application of the biochar to adsorb carbon dioxide. *Heliyon* 6: e04019. https://doi.org/10.1016/j.heliyon.2020.e04019
11. Sylvia N, Mutia R, Dewi R, et al. (2019) A computational fluid dynamic comparative study on CO_2 adsorption performance using activated carbon and zeolite in a fixed bed reactor. *IOP Conf Ser Mater Sci Eng* 536: 012042 https://iopscience.iop.org/article/10.1088/1757-899X/536/1/012042
12. Nouh S, Lau KK, Shariff AM (2010) Modeling and simulation of fixed bed adsorption column using integrated CFD approach. *J Appl Sci* 24: 3229-3235. 10.3923/jas.2010.3229.3235

13. Li S, Deng S, Zhao L, et al. (2018) Mathematical modeling and numerical investigation of carbon capture by adsorption: literature review and case study. *Appl Energy* 221: 437-449. 10.1016/j.apenergy.2018.03.093
14. Mesfer MKA, Danish M, Khan MI, et al. (2020) Continuous fixed bed CO_2 adsorption: breakthrough, column efficiency, mass transfer zone. *Processes* 8: 1233. DOI:10.3390/pr8101233
15. Sylvia N, Dewi R, Aprilia B, et al. (2023) Simultaneous fine particulate matter separation and CO_2 adsorption in a cyclone separator with a fixed bed bottom ash from a palm oil mill boiler: a simulation study. *Math Model Eng Probl* 10: 597-604. https://doi.org/10.18280/mmep.100229
16. Akpasi SO, Isa YM (2022) Effect of operating variables on CO_2 adsorption capacity of activated carbon, kaolinite, and activated carbon–Kaolinite composite adsorbent. *Water-Energy Nexus* 5: 21-28. https://doi.org/10.1016/j.wen.2022.08.001
17. Shafeeyan MS, Daud WM, Shamiri A, et al. (2015) Modeling of carbon dioxide adsorption onto ammonia-modified activated carbon: kinetic analysis and breakthrough behavior. *Energy Fuels* 29: 6565-6577. https://doi.org/10.1021/acs.energyfuels.5b00653.
18. Kan X, Chen X, Shen Y, et al. (2019) Box-Behnken design based CO_2 co-gasification of horticultural waste and sewage sludge with addition of ash from waste as catalyst. *Appl Energy* 242: 1549-1561. https://doi.org/10.1016/j.apenergy.2019.03.176
19. Dupre KR, Vyas A, Goldfarb JL, et al. (2019) Investigation of computational upscaling of adsorption of SO_2 and CO_2 in fixed bed columns. *Adsorption* 25: 773-782. https://doi.org/10.1007/s10450-019-00050-4
20. Umenweke GC, Afolabi IC, Epelle EI, et al. (2022) Machine learning methods for modeling conventional and hydrothermal gasification of waste biomass: A review. *Bioresour Technol Rep* 17: 100976. https://doi.org/10.1016/j.biteb.2022.100976
21. Yang H, Li W, Liu J, et al. (2019) Polyethylenimine-impregnated resins: The effect of support structures on selective adsorption for CO_2 from simulated biogas. *Chem Eng J* 35:822-829. https://doi.org/10.1016/j.cej.2018.08.220
22. Gorbounov M, Petrovic B, Ozmen S, et al. (2023) Activated carbon derived from Biomass combustion bottom ash as solid sorbent for CO_2 adsorption. *Chem Eng Res Des* 194: 325-343. https://doi.org/10.1016/j.cherd.2023.04.057
23. Liang F, Wei S, Wu L, et al. (2023) Improving the value of CO_2 and biogas slurry in agricultural applications: A rice cultivation case. *Environ Exp Bot* 208: 105233. https://doi.org/10.1016/j.envexpbot.2023.105233

AIMS Press